Phase diagram of cholesteric liquid crystals in a field

R. Seidin and D. Mukamel
Department of Physics of Complex Systems, Weizmann Institute of Science, 76100 Rehovot, Israel

D. W. Allender
Department of Physics and Liquid Crystal Institute, Kent State University, Kent, Ohio 44242

(Received 17 March 1997)

The phase diagram of a bulk cholesteric liquid crystal in an electric or magnetic field applied perpendicular to the pitch axis is studied. This is an example of a system which exhibits different types of phase transitions between various modulated and homogeneous states. Possible transitions are of three types: (1) first order, (2) continuous and described as a condensation of solitons with repulsive interaction, or (3) continuous but characterized by a small order parameter. The detailed behavior of the temperature-field phase diagram is found to be strongly dependent on the intrinsic chirality, where the existence of an undulating state is predicted at high chirality. The relevant temperature, electric field, and chirality ranges are experimentally attainable. [S1063-651X(97)00308-5]

PACS number(s): 61.30.Gd, 64.70.Md, 61.30.Cz

I. INTRODUCTION

Phase transitions in systems which exhibit modulated structures have been of interest for a long time due to their frequent appearance in a wide variety of physical systems. The transitions from modulated to homogeneous states can be of different types and involve various types of critical points (multicritical, tricritical, etc.). A particular example of such a system, where some of these features manifest themselves, is that of a cholesteric liquid crystal upon which a magnetic or electric field is applied. The behavior of a bulk cholesteric liquid crystal in the presence of an external field is of importance for many practical applications as well as for basic physical research. In this work we investigate the behavior of a bulk cholesteric system in an externally applied field within the context of phase transitions between modulated and homogeneous structures.

Continuous phase transitions from modulated to homogeneous states can be realized via two different mechanisms. The ordinary second-order transition involves some small order parameter which vanishes continuously at the transition. This type of transition is referred to as an *instability-type transition* [1]. However, another type of continuous transition which is not associated with a small order parameter is possible. This type is described by nucleation of solitons. The solitons arise as the domain walls separating regions of homogeneous states. In the domain wall region the perturbation of the homogeneous phase is not small, and thus a small local order parameter cannot be defined. The distance between solitons increases as the transition is approached, and becomes infinitely large at the transition point. These transitions are referred to as *nucleation transitions* [1–4]. A model for the homogeneous-modulated transition in magnetic systems, in which both kinds of continuous phase transitions are present along the phase boundary, was studied by Schaub and Mukamel [5]. The phase diagram of this model exhibits a transition line consisting of three segments: two of these correspond to the two types of continuous transitions (instability and nucleation types). They are separated by the third segment, which is first order. The two critical points at the two ends of the first-order segment are different in character: one is a usual tricritical point, separating the first-order segment from the instability-type segment, and the other is a multicritical point, which separates the first-order segment from the nucleation-type segment.

A bulk cholesteric liquid crystal which is subjected to a magnetic or electric field is also a system which exhibits a continuous phase transition of a nucleation type. When the external field is applied perpendicularly to the helical axis, at low temperatures, it unwinds the helical structure of the cholesteric state via a nucleation-type transition [6–8]. However, the cholesteric liquid crystalline system differs from the magnetic system in other features and these differences lead to a very different global phase diagram. For example, unlike magnetic helical systems, the zero-field transition to the disordered state in cholesteric liquid crystals is first order. This is due to the extra term in the Landau free energy, cubic in the order parameter, which is allowed by symmetry in the cholesteric case but is absent in the model which describes the magnetic system. Within the approach pursued in this work, the state of the system is determined by three parameters: temperature, field, and the intrinsic chirality of the cholesteric. Certain regions of the phase diagram in this three-dimensional space have been studied in the past [7–13]. Here we use the mean field approximation to study the global phase diagram and the nature of the resulting phase transitions. In this work, we study a model which describes the behavior of a bulk cholesteric liquid crystal subject to an applied magnetic or electric field normal to the helical axis. As discussed by Refs. [6,8], in bulk materials, if the field is initially applied in a different direction, the helical axis reorients to be perpendicular to the field. In restricted geometries, boundary effects may compete with the axis realignment, resulting in interesting reorientation transitions (see, for example, [14,15] and the references they contain). In this paper we do not consider boundary effects. We also do not consider blue phase structures, which arise in systems with high chirality. Three distinct types of states are found: a

nematic state (which may be either strongly or weakly ordered), a cholesteric modulated state with a nonvanishing winding number, and an undulating state, in which the director undulates periodically around the magnetic field direction. These states are characterized by different forms of the two scalar order parameters, referred to as the nematic and the phase order parameters. The nematic order parameter, which indicates the degree of orientational ordering in the system, is small in the weakly ordered nematic state and larger in the strongly ordered nematic state. The phase order parameter is constant in the nematic state, a bounded periodic function in the undulating state, and an unbound increasing (or decreasing) function in the cholesteric state.

The cholesteric phase diagram is very different from that found by Schaub and Mukamel for magnetic systems. The global phase diagram, in the temperature–applied-field plane varies as the intrinsic chirality of the system is changed. This parameter is tunable in our model and has different physical values for different cholesteric liquid crystalline materials. We found that cholesteric liquid crystals exhibit several types of phase transitions between the various available states and different types of critical and multicritical points.

The phase diagram and the various critical and multicritical points found in this study may readily be tested experimentally. Estimates of the relevant temperature, electric field, and chirality ranges (to be discussed in Sec. IV) at which many of the interesting features of the phase diagram are expected to take place indicate that they are experimentally attainable. In experimental studies of the temperature–electric-field phase diagram of the nematic materials 4-cyano-4'-(*n*-heptyl)biphenyl (7CB) [16] and 4'-*n*-pentyl-4-cyanobiphenyl (5CB) [17] it was found that the nematic-paranematic critical point is reached at $E \lesssim 250$ kV/cm and at $E = 141$ kV/cm, respectively. By, for example, mixing 5CB with a chiral liquid crystal, the system will become cholesteric. The interesting features of the resulting phase diagram are expected to take place at fields below or around 150 kV/cm.

The organization of this paper is as follows. In Sec. II we derive the rescaled model out of the free energy of a cholesteric liquid crystal subjected to an external field applied perpendicularly to the pitch axis. One has to solve explicitly the resulting equations of motion, but since we were not able to do this analytically we solved them numerically. Approximate analytical tools were also applied in order to gain more understanding of the mechanisms underlying the phase diagram. In Sec. III we present the complete mean field phase diagram, in the temperature-field plane, for different values of the intrinsic chirality obtained by both analytical and numerical means. The analytical results were obtained by using a reasonable, phase-only, approximation in which only the phase order parameter was allowed to vary in space. The accurate numerical results were obtained by solving numerically the coupled nonlinear Euler-Lagrange differential equations for the two order parameters with appropriate boundary conditions. In Sec. IV we summarize the main results and discuss the experimental implications of this study.

II. MODEL

In this section we consider the Landau theory of cholesteric liquid crystals. The appropriate macroscopic description of the cholesteric uses a symmetric traceless second-rank tensor, Q_{ij}, for example, the anisotropic part of the magnetic susceptibility tensor. The free energy density of a bulk cholesteric liquid crystal in the presence of an external magnetic field **H** can be described by the following Landau expansion [18–20]:

$$f_{\rm chol} = \frac{1}{2} A Q_{ij} Q_{ji} - \frac{1}{3} B Q_{ij} Q_{jk} Q_{ki} + \frac{1}{4} C (Q_{ij} Q_{ji})^2 + \tilde{q}_0 \epsilon_{ijk} Q_{il} Q_{kl,j} + \frac{1}{2} L_1 Q_{ij,k} Q_{ij,k} + \frac{1}{2} L_2 Q_{ij,i} Q_{kj,k} - \frac{1}{2} \chi_a^M H_i Q_{ij} H_j . \quad (1)$$

As usual, the coefficient A is taken to vary linearly with the temperature $A = a(T - T^*)$, where a and T^* are constants. The other coefficients, B, C, $\tilde{q}_0$, L_1, and L_2, are taken to be temperature independent. Here, ϵ_{ijk} is the completely antisymmetric third-rank tensor, $Q_{ij,k} \equiv \partial Q_{ij}/dx_k$, and the summation over repeated indices is being used. The molecular magnetic anisotropy χ_a^M is assumed to be positive, so that the magnetic field tends to align the liquid crystalline molecules along the field direction. The case of an electric field **E** is described by the substitution $\chi_a^M H_i Q_{ij} H_j \rightarrow [\epsilon_a^M/(4\pi)] E_i Q_{ij} E_j$ where ϵ_a^M is the molecular anisotropy of the dielectric permittivity.

The expansion (1) includes all terms allowed by symmetry, up to fourth order in Q_{ij} and quadratic order in its derivatives. The chiral nature of the cholesteric system results in the pseudoscalar first-order spatial derivative term in the free energy. Without loss of generality, the sign of $\tilde{q}_0$ is taken to be positive, corresponding to a right-handed chiral state.

It is well known that the tensor order parameter Q_{ij} which minimizes the free energy (1) in the cholesteric state has some degree of biaxiality. However, for long wavelength, i.e., small $\tilde{q}_0$, this biaxiality is small [21,22]. For simplicity the biaxiality is neglected in the present study, considering only a uniaxial order parameter Q_{ij}. In this case Q_{ij} can be written as

$$Q_{ij} = \frac{1}{2} S (3 n_i n_j - \delta_{ij}), \quad (2)$$

where $\mathbf{n} = (n_x, n_y, n_z)$ is a unit vector and S is the magnitude of the order parameter. In the geometry which is considered here **n** is assumed to be a planar vector: $\mathbf{n} = \mathbf{x}\cos\Theta + \mathbf{y}\sin\Theta$, **x** and **y** being two unit vectors perpendicular to the helical axis and perpendicular to each other. Using this form of the order parameter in Eq. (1) we get the following expression for the free energy:

$$f_{\rm chol} = \frac{3}{4} A S^2 - \frac{1}{4} B S^3 + \frac{9}{16} C S^4 - \frac{9}{4} \tilde{q}_0 S^2 \partial_z \Theta + \frac{9}{4} L S^2 (\partial_z \Theta)^2 + \frac{9}{16} L (\partial_z S)^2 - \frac{1}{8} \chi_a^M H^2 S - \frac{3}{8} \chi_a^M H^2 S \cos 2\Theta , \quad (3)$$

where we take, for simplicity, $L_1=-2L_2/3\equiv L$. This free energy is checked to be insensitive to the ratio of L_2/L_1 for values ranging from $-3/2$ up to 10. The number of free parameters can be reduced by rescaling the expression for the free energy density, using the following relations:

$$S=\frac{1}{3}\frac{B}{C}\phi, \quad \Theta=\frac{1}{2}\theta, \quad A=\frac{1}{6}\frac{B^2}{C}r,$$

$$z=\xi\zeta, \quad \xi^2=\frac{9}{2}\frac{CL}{B^2}, \quad \chi_a^M H^2=\frac{2}{9}\frac{B^3}{C^2}v,$$

$$\tilde{q}_0=\frac{L}{\xi}q_0, \quad f_{\rm chol}=\frac{1}{36}\frac{B^4}{C^3}\mathcal{F}. \tag{4}$$

Note that r may be written as $\tau(T-T^*)$ where $\tau=6Ca/B^2$. The resulting rescaled free energy takes the form

$$\mathcal{F}=-\frac{1}{3}v\phi+\frac{1}{2}r\phi^2-\frac{1}{3}\phi^3+\frac{1}{4}\phi^4-v\phi\cos\theta-q_0\phi^2\theta'$$
$$+\frac{1}{2}\phi^2(\theta')^2+\frac{1}{2}(\phi')^2. \tag{5}$$

It is described by three parameters r, v, and q_0, where r is proportional to the reduced temperature, v is proportional to the magnetic or electric field squared, and q_0 is the intrinsic chirality parameter which is related to the zero-field pitch, as discussed in Sec. IV. The prime denotes differentiation with respect to the reduced coordinate ζ. This is a one-dimensional model, where the pitch is parallel to ζ. We assume that the magnetic or electric field is applied in a direction perpendicular to the helical axis.

The main difference between this free energy density and that of the magnetic system studied in [5] is the existence of the cubic term $-\phi^3/3$ and the linear term $-v\phi/3$ in Eq. (5). It should be noted that compared to the magnetic system, this results in an extra tunable parameter, the rescaled intrinsic chirality q_0. The phase diagram and the nature of the various transition lines and critical points are found to be strongly dependent on q_0.

The equilibrium state of the system is described by the two rescaled functions $\phi(\zeta)$ and $\theta(\zeta)$. These functions are determined by the minimization of the functional associated with Eq. (5) with respect to both $\phi(\zeta)$ and $\theta(\zeta)$. This minimization results in the following Euler-Lagrange equations:

$$\phi''=r\phi-\phi^2+\phi^3-v\cos\theta-\frac{1}{3}v-2q_0\phi\theta'+\phi(\theta')^2, \tag{6a}$$

$$\phi^2\theta''=v\phi\sin\theta+2q_0\phi\phi'-2\phi\phi'\theta'. \tag{6b}$$

In order to get the full phase diagram in the (r,v,q_0) space, one has to solve these equations, subject to the appropriate boundary conditions. The resulting (r,v) phase diagram is presented in Figs. 1–3, for three different values of q_0. The following states were found to be stable in some regions of this phase space: the nematic N (or paranematic P) state, which is characterized by a constant ϕ and $\theta=0$,

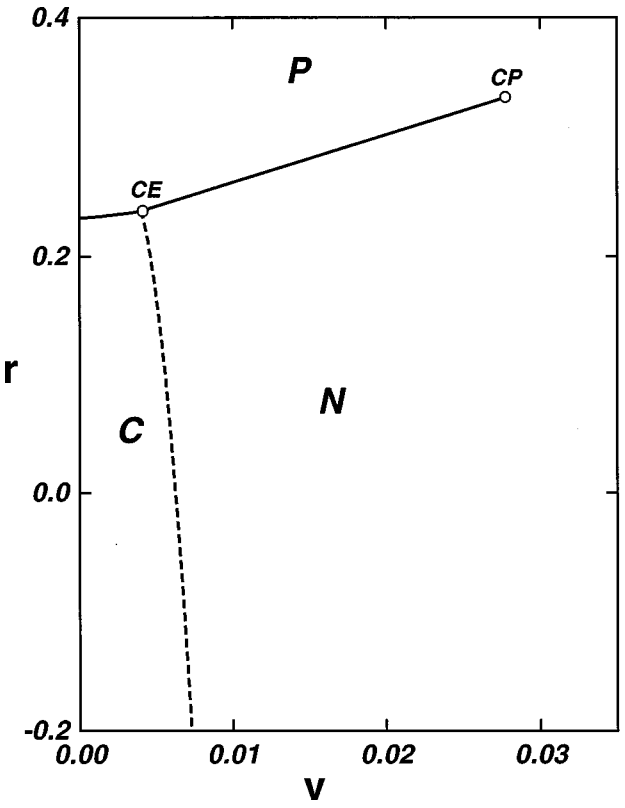

FIG. 1. The (r,v) phase diagram for the $q_0=0.1$, obtained numerically, as described in the text. Here and in the following phase diagrams solid lines represent first-order phase boundaries and dashed lines correspond to continuous phase boundaries. The cholesteric, nematic, and paranematic states are denoted by C, N, and P, respectively. The critical point and the critical end point are denoted by CP and CE, respectively. The approximate nucleation transition line (unshown) given by Eq. (8) is shifted to the left by $\Delta v/v\approx 0.008$ compared to the numerical line.

the modulated cholesteric state C which is characterized by a periodic nematic order parameter $\phi(\zeta)$ and an *unbound* increasing phase variable $\theta(\zeta)$, and an undulating state U, which is characterized by periodic $\phi(\zeta)$ and a *bound* periodic phase variable $\theta(\zeta)$.

The nematic state occurs at the high v, low r region of the phase diagram, the paranematic state at low v, high r, and the cholesteric state at low v, low r. At high temperatures when no field is applied upon the system, the cholesteric order is either metastable or unstable, and the system becomes isotropic via a first-order phase transition. When a field is switched on, it weakly orders the system to form a paranematic state. At lower temperatures the field distorts the helical structure of the cholesteric state, until it is completely unwound at some critical value of the field, at which the system exhibits a phase transition to a nematic state which is ordered in the direction of the field. For high enough chirality, the undulating state develops near the paranematic-nematic critical point, which is at high v, high r.

III. MEAN FIELD PHASE DIAGRAM

The various states which are realized in this model (nematic, cholesteric, and undulating) occupy different regions in the temperature-field (r,v) phase diagram. These regions are

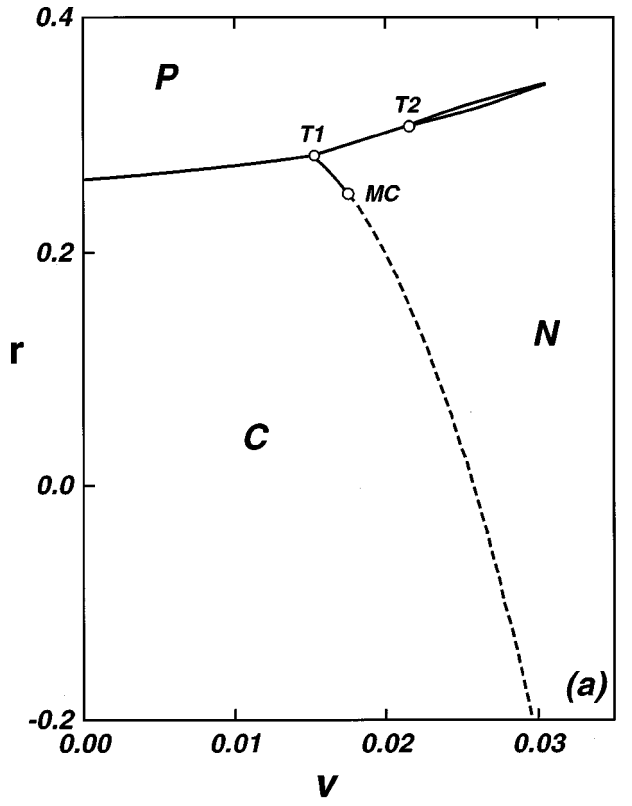

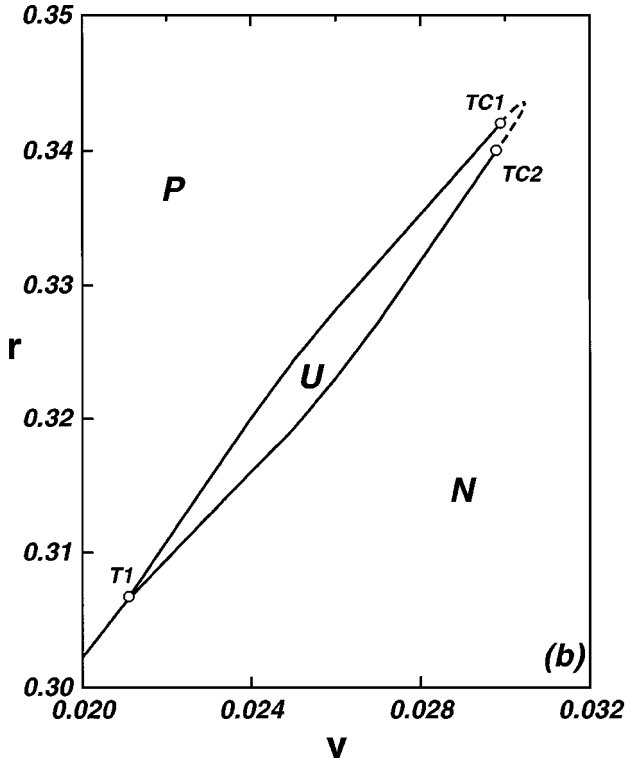

FIG. 2. (a) The (r,v) phase diagram for $q_0=0.2$. The multicritical point is denoted by MC and the triple points by $T1$ and $T2$. In (b) the region of the undulating state (U) is enlarged. The tricritical points are denoted by TC1 and TC2. The dashed line represents the analytical continuous instability line, and the solid lines correspond to the first-order transition lines, calculated numerically. The approximate nucleation transition line (unshown) is shifted to the left of the numerical line by 2%.

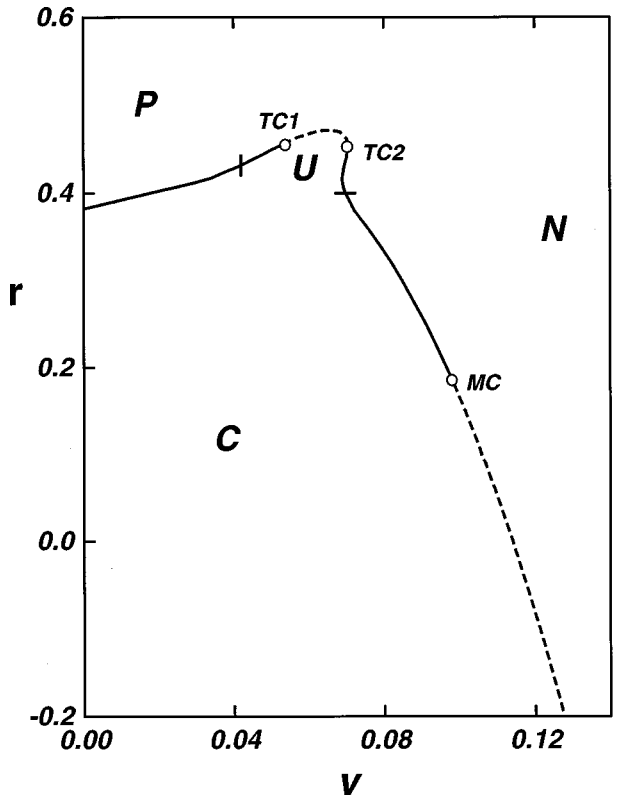

FIG. 3. The (r,v) phase diagram for $q_0=0.4$. The two bars represent the points on the transition line at which θ changes from being unbound to being bound. The approximate nucleation transition line (unshown) is shifted to the left of the numerical line by 4.5%.

separated by phase transition lines of several types. The detailed phase diagram strongly depends on the intrinsic chirality parameter q_0. We first summarize the main features of the phase diagram and the structure of the associated states, and then discuss their derivation. We also comment on the effect of fluctuations on the critical behavior associated with the various lines of second-order transitions occurring in the phase diagram.

For small q_0, the typical phase diagram is shown in Fig. 1. It exhibits a cholesteric state for small v and r. This state is separated from the paranematic and nematic region by two transition lines. One is a first-order transition line and the other is a continuous, nucleation-type, transition line. The two lines meet at a critical end point CE. The first-order line extends beyond the critical end point, separating a weak nematic (or paranematic) state from a strong nematic state. This line (referred to as the N-P line) ends at a liquid-gas-like critical point CP.

As q_0 increases beyond a critical value q_0^c, the nucleation line changes its character and becomes first-order at large r. The two resulting segments (first and second order) of the nucleation line are separated by a multicritical point MC. This point is not an ordinary tricritical point but rather a point at which the interaction between solitons changes from repulsive (in the second-order segment) to attractive (in the first-order segment). The first-order segment of the nucleation line meets the N-P line at a triple point, denoted as $T1$ in Fig. 2(a). For q_0 larger than another critical value q_0^u (which numerically is close to the estimated q_0^c), the nematic

state becomes unstable to undulations around the field direction, in some region near the critical point CP. This is shown in Figs. 2(a) and 2(b). The region occupied by the undulating state is bounded by a transition line which forms a closed loop, consisting of a continuous (instability-type) segment, that changes into first-order segments at each end via two ordinary tricritical points TC1, TC2. These first-order transition lines meet the *N-P* line at a triple point T2.

The region in which the undulating state is stable becomes larger as the intrinsic chirality q_0 is increased. For larger q_0 the region occupied by the undulating state approaches the cholesteric region, until they merge, forming a single region. Note that the cholesteric and the undulating states have the same symmetry, and therefore may exist as a single state in some region of the phase diagram. There exists, however, a line inside this region, separating the domain in which the phase order parameter is unbound (cholesteric state) from that in which it is bound (undulating state). On this line the nematic order parameter ϕ develops a set of nodes which allows for phase slip of the θ variable. This line is not a line of phase transitions, and no singularity of the free energy takes place on it. This phase diagram is shown in Fig. 3. Here, the cholesteric (or undulating) state is separated from the nematic (or paranematic) state by a line composed of four segments. In the order of increasing v they are first order, continuous instability type, another first order and a continuous nucleation type. The instability line is separated from the two first-order segments by two tricritical points TC1 and TC2. The nucleation line is separated from the first-order segment by a multicritical point MC.

In the following, we present some approximate analytical approaches for studying certain features of the phase diagram. The full phase diagram is then studied numerically.

A. The constant ϕ approximation

Analytical solutions of Eqs. (6) are not available. In order to get some understanding of the phase diagram it is instructive to find some approximate analytical solutions of these equations. A reasonable such approximation is the one in which the nematic variable ϕ is assumed to be a constant, letting only the phase θ be ζ dependent. This approximation is valid at the limit $v=0$ and it is improved for $v\neq 0$ as the intrinsic chirality of the system is reduced. We use this approximation to obtain a qualitative phase diagram for the model (5).

1. The N-P transition

In the region where the cholesteric helical structure is unwound ($\theta=0$) the system is described by a single order parameter ϕ which becomes independent of space. The free energy density takes the form

$$\mathcal{F}=\frac{1}{2}r\phi^2-\frac{1}{3}\phi^3+\frac{1}{4}\phi^4-\frac{4}{3}v\phi. \tag{7}$$

$\phi=\phi_0$ minimizes this free energy and satisfies the following cubic equation:

$$r\phi_0-\phi_0^2+\phi_0^3-\frac{4}{3}v=0. \tag{8}$$

In a nematic system ($q_0=0$), at zero field ($v=0$), there is a first-order transition between a disordered high temperature state and an ordered uniaxial nematic state. This transition takes place at $r=2/9$. When a chirality is introduced into the system ($q_0=0$), the transition temperature is shifted upwards, to $r=2/9+q_0^2$. This transition takes place between a disordered high temperature state and a cholesteric lower symmetry state.

When a field is switched on ($v>0$), the disordered state turns into a weakly ordered nematic state. It is easy to calculate, in the nematic region, the transition line from a high temperature weakly ordered (paranematic) state to a low temperature strongly ordered (nematic) state. The field dependent nematic-paranematic (N-P) transition temperature is given by

$$r=4v+\frac{2}{9}. \tag{9}$$

This transition line ends at the critical point, denoted by CP in Fig. 1 ($r_c=1/3$, $v_c=1/36$), which corresponds to $\phi_c=1/3$. This transition is of course suppressed in the region where the cholesteric state is energetically preferred. The cholesteric-paranematic transition in the presence of a field is also of first order, but it takes place at temperatures which are higher than in the nonchiral system. This segment has to be calculated numerically.

2. The nucleation line

Another transition line which can be derived in the phase-only approximation is the cholesteric-nematic unwinding transition line [7,8]. Near the nucleation transition, in the limit where the distance between domain walls is large, the translational behavior of the phase variable θ is $\theta(\zeta+2l)=\theta(\zeta)+2\pi$, and the amplitude ϕ is given by the nematic solution ϕ_0 obtained from Eq. (8). Treating l as an undetermined parameter, the free energy difference between the periodic and nematic states for a cell of thickness $2l$ (i.e., one period) has the following form to leading order in $1/l$ [7,8,23]:

$$F_\theta(l)=\frac{C_1}{l}+\frac{C_2}{l}e^{-2\gamma l}. \tag{10}$$

Here $C_1=\phi_0^2[4\gamma-\pi q_0]$, $C_2=16\phi_0^2\gamma$, and $\gamma=\sqrt{v/\phi_0}$. The first term may be interpreted as the energy per soliton, and the second term is the intersoliton *repulsive* interaction energy ($C_2>0$). In equilibrium, the distance between the domain walls, $2l$, is determined by minimizing $F_\theta(l)$ with respect to l. For $C_1>0$ the minimum is obtained at $l=\infty$, resulting in a nematic phase. However, for $C_1<0$, the minimum is obtained at $l\approx-(1/2\gamma)\ln(-C_1)$ with a logarithmic divergence of l as the transition is approached. Thus the nucleation transition occurs when $C_1=0$, i.e., at

$$v=\frac{\pi^2}{16}q_0^2\phi_0. \tag{11}$$

Using this result in Eq. (8), it is found that

$$\phi_0=\frac{1}{2}\left(1+\sqrt{1+\frac{\pi^2}{3}q_0^2-4r}\right). \tag{12}$$

Within the phase-only approximation, the nucleation transition line in the (r,v) plane is given by Eqs. (11) and (12).

The effect of fluctuations on nucleation transitions has been considered previously [24]. It has been shown that in $d=3$ dimensions (as in our case) fluctuations do not change the nature of the transition, and the logarithmic divergence of l persists beyond mean field.

B. The multicritical point

The interaction between solitons near the nucleation transition line, within the phase-only approximation, is always repulsive ($C_2>0$), resulting in a continuous transition. However, we will show that when the asymptotic behavior of ϕ at large ζ is taken into account, the interaction between solitons is always positive for small q_0, but for q_0 greater than a critical value q_0^c, the interaction C_2 is negative at small v and positive only at large v. When $C_2<0$, a chain of solitons forms and the transition is first order [5,25]. The first-order segment of the nucleation line and the cholesteric–weak-nematic transition line meet the *N-P* line at the triple point $T1$, as is shown in Fig. 2(a).

In order to determine the point at which the intersoliton interaction changes from repulsive to attractive, the asymptotic behavior of both ϕ and θ at large distances from the center of the soliton has to be determined for single soliton solutions. It is useful to locate the center of a soliton at the origin by making the transformation $\overline{\zeta}=\zeta-l$. Then, as $l\to\infty$, the limiting values of $\phi(\overline{\zeta})$ and $\theta(\overline{\zeta})$ are

$$\phi(\pm\infty)=\phi_0, \quad \theta(-\infty)=0, \quad \theta(\infty)=2\pi, \tag{13}$$

where ϕ_0 is the value of ϕ which minimizes the nematic free energy given in Eq. (7). Since we are looking far away from $\overline{\zeta}=0$, we may expand $\phi(\overline{\zeta})$ and $\theta(\overline{\zeta})$ around their limiting values:

$$\phi(\overline{\zeta})=\phi_0+\tilde{\phi}(\overline{\zeta}), \tag{14a}$$

$$\theta(\overline{\zeta})=\begin{cases}\tilde{\theta}(\overline{\zeta}), & \overline{\zeta}\ll 1\\ 2\pi+\tilde{\theta}(\overline{\zeta}), & \overline{\zeta}\gg 1.\end{cases} \tag{14b}$$

The linearized equations of motion which result from the insertion of Eq. (14) into Eq. (6) are

$$\tilde{\phi}''+2q_0\phi_0\tilde{\theta}'-(r-2\phi_0+3\phi_0^2)\tilde{\phi}=0, \tag{15a}$$

$$\phi_0^2\tilde{\theta}''-2q_0\phi_0\tilde{\phi}'-v\phi_0\tilde{\theta}=0. \tag{15b}$$

It is sufficient to examine the $\overline{\zeta}\to\infty$ limit since $\overline{\zeta}\to-\infty$ leads to the same result.

Let $\tilde{\phi}=A_\phi\exp(-\alpha\overline{\zeta})$, $\tilde{\theta}=A_\theta\exp(-\alpha\overline{\zeta})$ where A_ϕ and A_θ are constants. Inserting this ansatz into the linearized equations of motion, one gets an algebraic set of equations for A_ϕ and A_θ:

$$\begin{pmatrix}\alpha^2-(r-2\phi_0+3\phi_0^2) & -2q_0\phi_0\alpha\\ 2q_0\phi_0\alpha & \phi_0^2\alpha^2-v\phi_0\end{pmatrix}\begin{pmatrix}A_\phi\\ A_\theta\end{pmatrix}=0. \tag{16}$$

The condition for having a nontrivial solution to these equations is

$$\alpha^4-\alpha^2\left(\frac{v}{\phi_0}+r-2\phi_0+3\phi_0^2-4q_0^2\right)+3v\phi_0-2v+\frac{v}{\phi_0}r=0. \tag{17}$$

Whether α is real or complex depends on the values of the parameters. As argued by Jacobs and Walker [25], real α corresponds to a repulsive large-distance interaction between the domain walls, while complex α leads to an attractive large-distance interaction. The large-distance interactions, which are relevant when only a small number of solitons exist in the system, can be determined by using linear stability analysis around the asymptotic form (14) for $\phi(\overline{\zeta})$ and $\theta(\overline{\zeta})$. The interaction free energy $F_{\rm int}(r,v,\alpha)$ is the difference between the free energy of a chain of solitons ($F_{\rm chain}$) and the sum of all single soliton free energies ($F_{\rm single}$). It can be calculated at the unwinding transition using the asymptotic forms of $\phi(\overline{\zeta})$ and $\theta(\overline{\zeta})$, Eq. (14). For the case of complex α, $F_{\rm int}(r,v,\alpha)$ is negative at certain intersoliton distances, and the chains are favorable over the single soliton configuration. In this case, the interaction is attractive, and the transition from a nematic state to a cholesteric state is first order. If α is real, $F_{\rm int}(r,v,\alpha)$ is positive, and a chain configuration is not favored energetically. This situation describes repulsion between solitons and leads to a continuous transition.

The interaction between solitons changes from repulsive to attractive, at the point at which the discriminant D of Eq. (17) vanishes. This yields the following equation which should be satisfied by the multicritical point:

$$D=\left(\frac{v}{\phi_0}+r-2\phi_0+3\phi_0^2-4q_0^2\right)^2-4\left(3v\phi_0-2v+\frac{v}{\phi_0}r\right)=0. \tag{18}$$

We then assume that the multicritical point lies on the nucleation line, as given by the phase-only approximation, so that its coordinates are determined by a simultaneous solution of Eqs. (18), (8), and (11). The second equation determines ϕ_0 for given v and r, and the third one determines the intersection point of the locus of points at which the interaction changes from repulsive to attractive with the nucleation line. There are only two points in the (r,v) plane which satisfy all three equations (18), (8), and (11). They are given by

$$r_M^{(\pm)}=(\phi_0^{M(\pm)})^2+\left(\frac{5\pi^2}{48}-(4\pm\pi)\right)q_0^2, \tag{19a}$$

$$v_M^{(\pm)}=\frac{\pi^2}{16}q_0^2\phi_0^{M(\pm)}, \tag{19b}$$

and they correspond to

$$\phi_0^{M(\pm)}=\tfrac{1}{4}[1+\sqrt{1+8(4\pm\pi-\pi^2/48)q_0^2}],$$

respectively.

For $q_0<q_0^c\approx 0.1434$ both points $(v_M^{\pm},r_M^{\pm})$ lie above the N-P transition line in the (r,v) plane; thus for these values of q_0 the cholesteric-nematic transition line stays continuous all the way up to the N-P transition line. For $q_0>q_0^c$, the point (v_M^{+},r_M^{+}) lies below the N-P transition line. This is the multicritical point at which the cholesteric-nematic nucleation transition changes from continuous to first order. At q_0^c, the meeting point of the first-order segment of the nucleation line and the N-P line changes its character from being a critical end point (as in Fig. 1) to being a triple point [as in Fig. 2(a)].

C. The undulating instability line

In the following, we determine the stability limits of the nematic state. We consider a situation in which the nematic state is periodically perturbed and study the conditions under which it is unstable against undulations.

It is convenient to represent the order parameters $\phi(\zeta)$ and $\theta(\zeta)$ in terms of the two real scalar functions $\phi_1(\zeta)$ and $\phi_2(\zeta)$: $\phi_1+i\phi_2=\phi e^{i\theta}$. We introduce a small order parameter ϵ, and expand $\phi_1(\zeta)$ and $\phi_2(\zeta)$ around the nematic state described by $\phi_1=\phi_0$, $\phi_2=0$. The nematic amplitude ϕ_0 satisfies Eq. (8) and minimizes the nematic free energy (7). To carry out this expansion we introduce the following ansatz for the fields ϕ_1 and ϕ_2 [5]:

$$\phi_1=\phi_0+\epsilon^2 A+\epsilon\sigma_1\cos(q\zeta)+\epsilon^2\beta_1\cos(2q\zeta)+O(\epsilon^3), \tag{20a}$$

$$\phi_2=\epsilon\sigma_2\sin(q\zeta)+\epsilon^2\beta_2\sin(2q\zeta)+O(\epsilon^3), \tag{20b}$$

where $\sigma_1^2+\sigma_2^2=1$ and the coefficients A, σ_1, β_1, β_2, and q have to be determined by a minimization of the free energy. We are interested in calculating the free energy to order ϵ^4 and therefore higher-order terms in the expressions for ϕ_1 and ϕ_2 need not be considered. Using this expansion, the free energy per unit length associated with Eq. (5) can be written as a power series in ϵ:

$$F=F_0+a_2\epsilon^2+a_4\epsilon^4+O(\epsilon^6). \tag{21}$$

This is a Landau-type expression for the free energy near a second-order transition expanded in the small order parameter ϵ. Here, F_0, given by Eq. (7), is the free energy of the nematic state characterized by a constant $\phi=\phi_0$. The second-order transition between the nematic state and the undulating state occurs when the coefficient of the quadratic term vanishes, i.e., $a_2=0$.

$$a_2=-\frac{v}{12\phi_0}\sigma_2^2+\frac{1}{4}r-\frac{1}{4}\phi_0(\sigma_1^2+1)+\frac{1}{4}\phi_0^2(2\sigma_1^2+1)$$
$$-q_0 q\sigma_1\sigma_2+\frac{1}{4}q^2. \tag{22}$$

The parameters σ_1, σ_2, and q are determined by minimizing a_2, subject to the constraint $\sigma_1^2+\sigma_2^2=1$, and they are given by

$$q=2q_0\sigma_1\sigma_2, \tag{23a}$$

$$\sigma_1^2=\frac{1}{2}\left[1-\frac{1}{2q_0^2}\left(\frac{v}{6\phi_0}-\frac{1}{2}\phi_0+\phi_0^2\right)\right], \tag{23b}$$

$$\sigma_2^2=\frac{1}{2}\left[1+\frac{1}{2q_0^2}\left(\frac{v}{6\phi_0}-\frac{1}{2}\phi_0+\phi_0^2\right)\right]. \tag{23c}$$

The expressions for σ_1 and σ_2 are not always physical. Requiring that σ_1^2 and σ_2^2 are non-negative we obtain the following condition:

$$\left|\frac{v}{6\phi_0}-\frac{1}{2}\phi_0+\phi_0^2\right|\leqslant 2q_0^2. \tag{24}$$

The minimal q_0 for which this condition is satisfied is $q_0^u=1/\sqrt{48}\approx 0.1443$. For $q_0=q_0^u$ the instability takes place at the critical point CP which ends the N-P line. For $q_0<q_0^u$ the condition (24) is not satisfied and the nematic state is stable to small perturbations. The predicted value of $q_0^u=0.1443$ is very close to the estimated value of $q_0^c=0.1434$ which was obtained in the preceding section using an asymptotic approximation. We have not done the extensive numerical calculation required to determine q_0^c precisely and thus determine which of the two critical wave vectors, q_0^c and q_0^u, is larger. For $q_0>q_0^u$ the instability line is physical, and there is a region in the (r,v) plane where the undulating state is stable. The $a_2=0$ line is stable as long as $a_4(\sigma_1,\sigma_2,q,A,\beta_1,\beta_2)\geqslant 0$. The expression for a_4 is rather lengthy and will not be explicitly presented here. After determining the parameters A, β_1, and β_2 by minimizing a_4 with respect to each one of them, and solving the equations $a_2=0$ and $a_4=0$, we find two distinct tricritical points for every $q_0>q_0^u$ [see Fig. 2(b)]. For values of v below the tricritical points, the transition to the undulating state is first order. At $q_0=q_0^u$ the critical point CP becomes a Lifshitz point [26,27]. The (r,v) phase diagram in the vicinity of this point is basically the phase diagram corresponding to a Lifshitz point in the presence of an ordering field. The first-order segment of the instability line is found numerically for several values of q_0. For $q_0\gtrsim q_0^u$ the undulating instability line is far from the triple point $T1$ (or from the critical end point CE), and it intersects the N-P line at a triple point $T2$, forming a closed loop. An example for this case can be seen in Fig. 2(b), for $q_0=0.2$. As q_0 is further increased, the region where the undulating state is stable increases, and its boundaries move towards the cholesteric region until they merge at $q_0\approx 0.25$. In this case, as is shown in Fig. 3 for $q_0=0.4$, the first-order cholesteric-paranematic transition and the first-order cholesteric-nematic transition continue smoothly the first-order segments of the instability line (the meeting points are denoted in Fig. 3 by bars).

The Landau-Ginzburg model corresponding to the second-order segment of the transition from the nematic to the undulating state is an X-Y-like model. It is thus expected that this transition belongs to the universality class of the $n=2$ component vector model.

D. Numerical results

As noted in the preceding section the Euler-Lagrange equations (6) obtained for the model (5) cannot be solved analytically. In the beginning of this section, we presented an approximate treatment of Eq. (5), in which only the phase order parameter θ was allowed to vary in space. We found an approximate expression for the nucleation line, Eqs. (11) and (12), and the multicritical point on this line, at which the nature of the cholesteric-nematic transition changes from continuous to first order. However, in order to obtain a more detailed phase diagram of model (5) the ζ dependence of ϕ must also be taken into account, and thus a numerical treatment of Eqs. (6) is needed. Equations (6) for $\phi(\zeta)$ and $\theta(\zeta)$ are solved numerically, employing a special code called COLNEW [28,29], which was specifically developed for solving multipoint boundary value problems for a coupled system of ordinary differential equations. We chose to rescale Eq. (5) by the length l ($2l$ is the periodicity of the modulated states), so that l becomes a parameter in the expression for the rescaled free energy, rather than in the limits of integration. The periodicity $2l$ and the chirality $q=\pi/l$ are determined at every point (v,r,q_0) in the phase diagram by a minimization procedure. For $v=0$, the actual chirality q is equal to the intrinsic chirality q_0. The rescaled Euler-Lagrange equations that were solved are

$$\frac{1}{l^2}\phi''+\frac{1}{3}v-r\phi+\phi^2-\phi^3+v\cos\theta+\frac{2}{l}q_0\phi\theta'-\frac{1}{l^2}\phi(\theta')^2=0, \tag{25a}$$

$$\frac{\phi}{l^2}\theta''-2q_0\phi\phi'+\frac{2}{l^2}\phi\phi'\theta'-v\phi\sin\theta=0, \tag{25b}$$

where the prime stands now for a derivative with respect to the dimensionless coordinate $\tilde{\zeta}=\zeta/l$. The rescaled boundary conditions that should be satisfied by ϕ and θ are

$$\phi'(0)=0, \quad \phi'(1)=0, \tag{26a}$$

$$\theta(0)=0, \quad \theta(1)=\pi \tag{26b}$$

for the cholesteric configuration, and

$$\phi'(0)=0, \quad \phi'(1)=0, \tag{27a}$$

$$\theta(0)=0, \quad \theta(1)=0 \tag{27b}$$

for the undulating configuration.

Equations (25) are solved for both sets of boundary conditions [Eqs. (26) and (27)] by employing the COLNEW procedure. Examination of the order parameter profiles and comparison between the energies of the different states enables us to determine the thermodynamic boundaries separating the different states in the phase diagram, and also to determine whether the phase transitions are of first or second order.

Both first- and second-order boundaries appear in the phase diagram. A point on the nematic side of the second-order nucleation transition line is found by reaching the first point at which the minimum of the free energy occurred at $q=0$. For a first-order case, the situation is different. It is determined by the first point for which there existed a $q=0$ solution of the Euler-Lagrange equations but the cholesteric (or the undulating) free energy is larger than the corresponding nematic one.

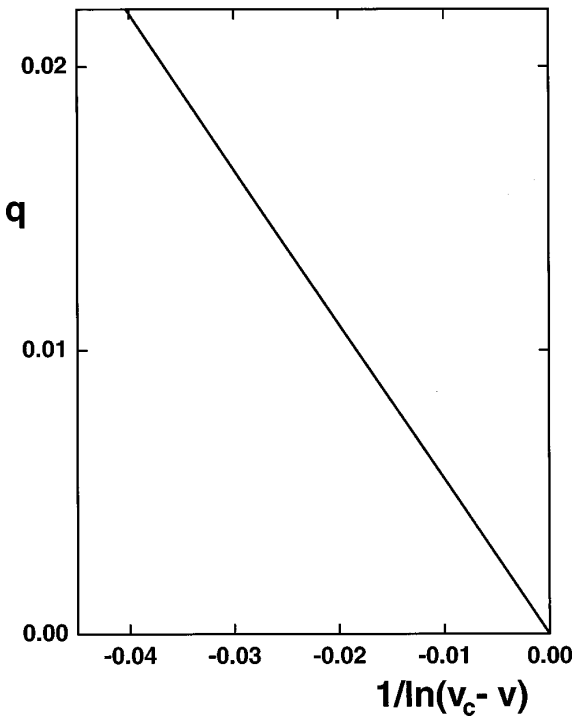

FIG. 4. The chirality wave vector q as a function of v, for $q_0=0.1$, along the cholesteric–weak-nematic transition line, as the critical end point CE is approached. The horizontal axis is chosen to be $1/\ln(v_c-v)$ ($v_c=0.004\,017\,67$), in order to show directly the behavior which was described in Sec. III A 2.

Note that the nematic solution ($q=0$, $\theta=0$, and $\phi=$const) is a trivial solution for the Euler-Lagrange equations, but it is not the thermodynamically stable solution outside the nematic region. The parameters at which the $q=0$ solution is replaced by the $q\neq 0$ one can then be determined only by comparing the free energies of the two solutions.

The results of the numerical solution are summarized graphically in Figs. 1–5. In Figs. 1–3 the complete phase diagrams for several values of q_0 are presented ($q_0=0.1$, which is below q_0^c and q_0^u, $q_0=0.2$ which is above both q_0^c and q_0^u, and $q_0=0.4$ which is far above q_0^c and q_0^u). These are the typical phase diagrams, corresponding to three different regimes of q_0. As a rule, the region occupied by the cholesteric state becomes larger as q_0 is increased, i.e., the cholesteric–weak-nematic transition occurs at higher temperatures and the cholesteric–strong-nematic transition takes place at higher values of the applied field. The cholesteric–weak-nematic transition temperature increases monotonically with the field, intersecting the r axis at $r=2/9+q_0^2$. For $q_0=0.1$ ($<q_0^c$), this line joins the N-P line smoothly while for $q_0=0.2$ ($>q_0^c$) the two lines intersect with a finite change in slope. In the case of $q_0=0.1$, the entire cholesteric-nematic transition is continuous (of a nucleation type). This line intersects the N-P line and the cholesteric–weak-nematic transition line at a critical end point CE. As the CE is approached along the cholesteric–weak-nematic line, q vanishes, as is shown in Fig. 4. The $q_0=0.2$ case is

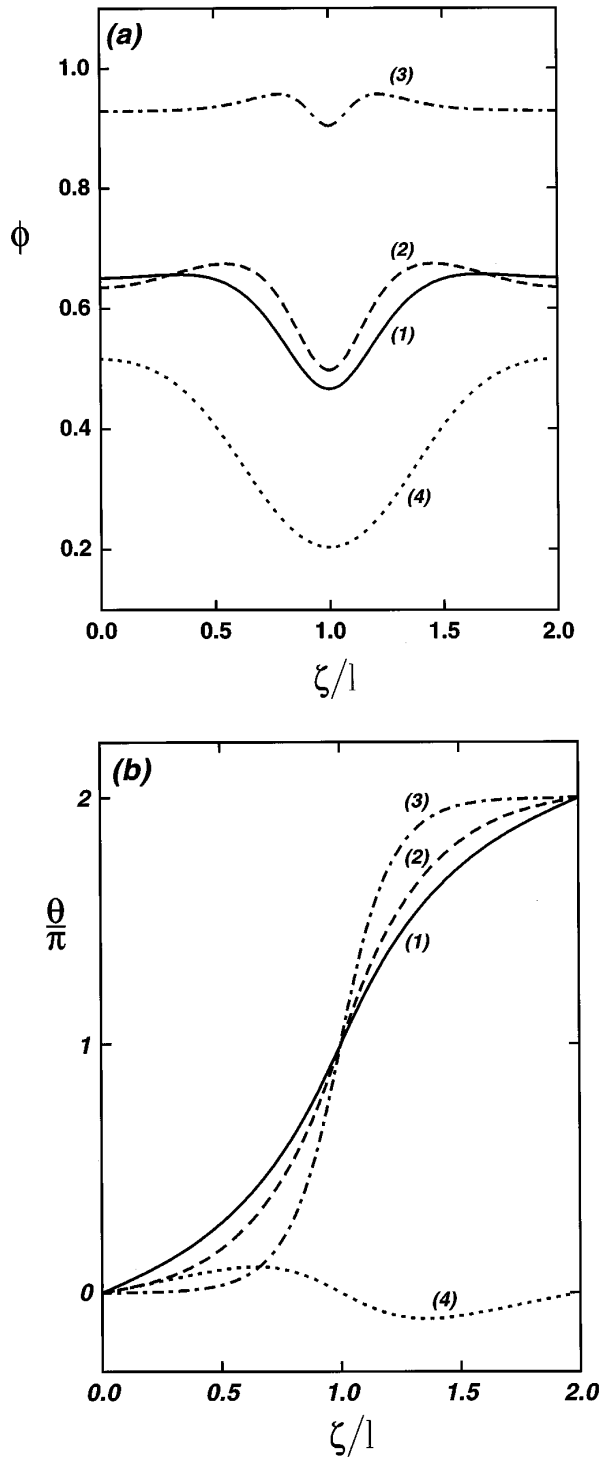

FIG. 5. In (a) and (b) the profiles of $\phi(\zeta/l)$ and $[\theta(\zeta/l)]/\pi$ are shown, respectively, at several points on the $q_0=0.2$ (r,v) phase diagram for one period $(0\leqslant\zeta/l\leqslant 2)$. The *solid* profiles (1) correspond to a point at the cholesteric-paranematic transition line $(v=0.0137,\ r=0.280,\ q=0.171)$. The *dashed* profiles (2) correspond to a point at the first-order segment of the nucleation line $(v=0.015\,83,\ r=0.275,\ q=0.133)$. The *dash-dotted* profiles (3) correspond to a point near the nucleation line $(v=0.0232,\ r=0.1,\ q=0.069)$. The *dotted* profiles (4) correspond to a point in the undulating region, near the first-order part of the instability transition line $(v=0.026,\ r=0.325,\ q=0.184)$. Note that in the cholesteric state (1)–(3) θ increases by 2π over a period while in the undulating state (4) θ is a periodic function.

different. The multicritical point $(v=0.0176,\ r=0.25)$ on the cholesteric-nematic transition line lies below the triple point, and thus the segment of this transition line which connects the multicritical point and the triple point is of first order. In this case q does not vanish at the triple point, but its value changes discontinuously. The cholesteric to strong nematic transition line is first order at the triple point $T1$ and the three transition lines which meet at this point must form three angles, each of which is smaller than 180°, according to the rule for the intersection of three first-order transition lines [30]. The multicritical point slides down along the cholesteric–strong-nematic transition line as q_0 is increased, and the first-order segment of this transition becomes longer, as can be seen by comparing the $q_0=0.2$ case in Fig. 2(a) to the $q_0=0.4$ case in Fig. 3.

As q_0 increases, the triple point $T1$ gets closer to the N-P critical point CP $(v_c=1/36,\ r_c=1/3)$. At the same time, the point at which the instability (to undulations) line closes on the N-P line $T2$ slides down in the opposite direction. For $q=0.2$ these two regions are well separated, as can be seen in Fig. 2(a). In Fig. 2(b) the detailed structure of the instability line for $q_0=0.2$ is shown. The dashed line which connects the two tricritical points represents a continuous transition, and the solid segments which meet on the N-P line correspond to first-order transitions. As q_0 is further increased, the distance between the two points $(T1)$ and $(T2)$ decreases, until they merge for $q_0\approx 0.25$. The precise mechanism of this merging process was not investigated in this study. For values of q_0 which are larger than 0.25 the global phase diagram changes. The cholesteric and the undulating states are no longer separated, but instead form a single modulated state. Naively, one would expect the two states to be separated, since their modulated structures seem to be topologically different [in one case $\theta(\zeta)$ is unbound while in the other it is bounded]. This would indeed be the case if $\phi(\zeta)>0$ for all ζ. However, if the amplitude ϕ vanishes at some point ζ, the winding number is no longer topologically meaningful, and one can go from one state to the other in a continuous fashion. The line in the (r,v) plane on which $\phi(\zeta)$ has a set of nodes can be calculated numerically. This line intersects the modulated-nematic transition lines at two points, which are denoted by bars in Fig. 3. In this figure, the $q_0=0.4$ phase diagram is given. In this diagram, the instability line consists of both second- (dashed) and first- (solid) order segments separated from each other by the two tricritical points TC1 and TC2. These first-order segments join onto the first-order cholesteric–weak-nematic line and the first-order continuation of the nucleation line. Along the cholesteric–weak-nematic and undulating instability lines q is finite and it varies smoothly along the line. The continuous instability transition occurs for finite q, as opposed to the nucleation-type transition at which q vanishes.

In Fig. 4 we present the behavior of q as a function of v for $q_0=0.1$ on the cholesteric-paranematic transition line, as the critical end point CE is approached. Clearly q goes to 0 and the transition at the critical end point is continuous. We plotted q versus $1/\ln(v_c-v)$ in order to show in a clear manner the expected logarithmic behavior near a continuous transition of a nucleation type.

In Fig. 5 we show characteristic profiles of the order parameters θ and ϕ near the transition lines for $q_0=0.2$. These

profiles yield the structure of the modulated states at different points near various transition lines. The solid and the dashed curves correspond to points near the first-order cholesteric–weak-nematic, and the first-order cholesteric–strong-nematic transition lines, respectively. The dash-dotted curves are associated with the order parameters very close to the nucleation transition, at which q vanishes. The dotted profiles correspond to the order parameters in the undulating region, where $\theta(\zeta)$ is bound, near the first-order part of the undulating-nematic transition, at which q stays finite.

IV. DISCUSSION

In this work, we studied the mean field phase diagram of a bulk cholesteric liquid crystal subjected to an externally applied field. The phase diagram was found to be rather rich, exhibiting two types of modulated states: a cholesteric state characterized by a nonvanishing winding number, and an undulating state in which the director makes small oscillations around the direction of the applied field. The nature of the transition lines separating the various states and the multicritical points at which these lines meet have been studied in detail. In the present study it was assumed that the system is described by a uniaxial order parameter. This assumption is valid for low chirality where the biaxial corrections are small, of order q^4. In the following, we discuss the experimental implications of this study and present estimates of the range of fields (either electric or magnetic), temperature, and chiralities at which some of the more interesting features of the phase diagram could be observed. It is found that while the magnetic field required to reach the critical point CP is very high (about 40 T), the required electric field is of the order of a few hundreds of kV/cm, which is within experimental reach.

Consider first the chirality q_0. It corresponds to a pitch P given by $P=4\pi\xi/q_0$, where ξ is the correlation length defined in Eq. (4). Taking 10 nm as a typical value of ξ [31] one gets $P=125/q_0$ nm. The interesting features of the phase diagram occur at q_0 in the range of $0.1-0.2$, corresponding to a pitch P in the range of 1260–630 nm, which is a comfortable experimental range. The wavelength λ of the backscattered light from a modulated structure is related to P via $\lambda=Pn$, where n is the refraction index of the liquid crystal. For a typical n of 1.6 the wavelength of the scattered light is expected to be in the range of 2000 nm to 1000 nm. In the present work we analyzed structures which are modulated in one direction only. More complicated structures such as those occurring in blue phases have not been considered. It has been shown [20] that such structures are expected to occur for chiralities $q_0 \gtrsim 0.28$ (note that the chirality parameter q_0 which is used here is related to the chirality parameter κ used in Ref. [20] by $q_0=\kappa/\sqrt{6}$). We therefore expect the interesting regions of the phase diagrams of Figs. 1–3 to be physically realizable.

We now turn to the question of the magnitude of the applied field for which the phenomena of interest are expected to take place. Consider a magnetic field first. The relation between the variable v and the corresponding magnitude of the magnetic field in Gaussian units is given by

$$H^2=\left(\frac{9\phi}{2}\frac{K_2}{\chi_A\xi^2}\right)v, \tag{28}$$

where $K_2=(4/9)(B^4\xi^2)/C^3$ is the twist elastic coefficient, typically of order 4×10^{-7} dyn, $\chi_A=(\phi B/C)\chi_A^M$ is the magnetic anisotropy, typically 10^{-7} in cgs units, and ξ, the correlation length, is typically of order 10^{-6} cm [6]. Using this relation, the critical applied field for the N-P transition, which in our dimensionless units is found at $v=1/36$ and $\phi=1/3$, corresponds to a value of the order of 400 kG, which is not easily accessible experimentally. Perhaps the critical field could be approached at national high magnetic field facilities. The corresponding magnitude of the electric field in statvolts/cm is given by

$$E=\sqrt{4\pi}\left(\frac{\chi_A}{\epsilon_A}\right)^{1/2}H, \tag{29}$$

where ϵ_A is the dielectric anisotropy, the value of which is typically in the range of 0.1–40, in cgs units. Using this relation, assuming $\epsilon_A=10$, we found that the critical electric field is 400 kV/cm, which is achievable experimentally, especially if pulsed field techniques are used. In experiments on the nematic material 4'-*n*-pentyl-4-cyanobiphenyl (5CB) in an electric field the critical point was found to occur at $E=141$ kV/cm, which is consistent with the crude estimate presented above.

Next we estimate the temperature range over which the undulating phase is expected to be stable. The rescaled temperature r is linearly related to the difference $(T-T^*)$ [see Eq. (4)] by $r=\tau(T-T^*)$. At the nematic-isotropic transition (NI), when no field is applied, $r_{\rm NI}=2/9$ corresponds to $(T_{\rm NI}-T^*)=1\ ^\circ$C, following de Gennes and Prost [32]. Thus $\tau=2/9\ (^\circ\text{C})^{-1}$, and at the NP critical point $(T_{\rm CP}-T^*)=3/2\ ^\circ$C, which is consistent with Ref. [16]. The undulating state for $q_0=0.2$ (pitch equal to 630 nm) is shown in Fig. 2 to have a width in r of about 0.005, which corresponds to 0.02 °C. This range is quite narrow, but it can be increased by using a smaller intrinsic pitch, or a larger $T_{\rm NI}-T^*$.

We summarize by emphasizing that the phenomena presented in this work, including the observation of the multicritical point and the undulating state, are expected to be observable in materials of intermediate pitch, with large ϵ_A and $T_{\rm NI}-T^*$, under conditions of careful temperature control and relatively high electric fields.

ACKNOWLEDGMENTS

This work was supported in part by the National Science Foundation under Science and Technology Center ALCOM Grant No. DMR 89-20147 and the Basic Research Foundation, administrated by the Israeli Academy of Arts and Sciences, Jerusalem, Israel. One of the authors (D.W.A.) acknowledges receiving financial support from the Weizmann Institute of Science as a Varon Visiting Professor.

[1] P.G. de Gennes, in *Fluctuations, Instabilities and Phase Transitions*, Proceedings of the NATO Advanced Study Institute, Geilo, Norway, edited by T. Riste (Plenum, New York, 1975).
[2] A.E. Jacobs and D. Mukamel, J. Stat. Phys. **58**, 503 (1990).
[3] A.E. Jacobs, G. Goldner, and D. Mukamel, Phys. Rev. A **45**, 5783 (1992).
[4] T. Ohyama, A.E. Jacobs, and D. Mukamel, Phys. Rev. E **53**, 2595 (1996).
[5] B. Schaub and D. Mukamel Phys. Rev. B **32**, 6385 (1985); J. Phys. C **16**, L225 (1983).
[6] P.G. de Gennes and J. Prost, *The Physics of Liquid Crystals* (Oxford, London, 1993).
[7] P.G. de Gennes, Solid State Commun. **6**, 163 (1968).
[8] R.B. Meyer, Appl. Phys. Lett. **14**, 208 (1969); **12**, 281 (1968).
[9] P. J. Kedney and I. W. Stewart, Lett. Math. Phys. **31**, 261 (1994).
[10] L. Gil, J. Phys. (France) II **5**, 1819 (1995).
[11] L. Longa, D. Monselesan, and H.R. Trebin, Liq. Cryst. **5**, 889 (1989).
[12] S.V. Shiyanovskii and J.G. Terentieva, Phys. Rev. E **49**, 916 (1994).
[13] E. Niggemann and H. Stegemeyer, Liq. Cryst. **5**, 739 (1989).
[14] F. Rondelez and J.P. Hulin, Solid State Commun. **10**, 1009 (1972).
[15] J.P. Hurault, J. Chem. Phys. **59**, 2068 (1973).
[16] A.J. Nicastro and P.H. Keyes, Phys. Rev. A **30**, 3156 (1984).
[17] I. Lelidas and G. Durand, Phys. Rev. E **48**, 3822 (1993).
[18] P.G. de Gennes, Mol. Cryst. Liq. Cryst. **12**, 193 (1971).
[19] G. Vertogen and W.H. de Jeu, *Thermotropic Liquid Crystals, Fundamentals* (Springer-Verlag, Berlin, 1988).
[20] R.M. Hornreich, M. Kugler, and S. Shtrikman, Phys. Rev. Lett. **54**, 2099 (1985).
[21] D.C. Wright and N.D. Mermin, Rev. Mod. Phys. **61**, 385 (1989).
[22] R.M. Hornreich and S. Shtrikman, Phys. Rev. A **29**, 3444 (1984).
[23] M. Luban, D. Mukamel, and S. Shtrikman, Phys. Rev. A **10**, 360 (1974).
[24] M.F. Fisher and D.S. Fisher, Phys. Rev. B **25**, 3192 (1982).
[25] A.E. Jacobs and M.B. Walker, Phys. Rev. B **21**, 4132 (1980).
[26] R.M. Hornreich, M. Luban, and S. Shtrikman, Phys. Rev. Lett. **35**, 1678 (1975).
[27] R.M. Hornreich, J. Magn. Magn. Mater. **15-18**, 387 (1980).
[28] U. Ascher, J. Christiansen, and R.D. Russel, ACM Trans. Math. Softw. **7**, 209 (1981).
[29] U. Ascher, R.M.M. Mattheij, and R.D. Russel, *Numerical Solution of Boundary Value Problems for Ordinary Differential Equations* (Prentice-Hall, Englewood Cliffs, NJ, 1988), pp. 486–490.
[30] J. Wheeler, J. Chem. Phys. **61**, 4474 (1974).
[31] Reference [20] uses a correlation length of 25 nm, but our definition in Eq. (4) is smaller than theirs by a factor of $1/\sqrt{6}$.
[32] See, for example, Ref. [6], p. 87.